

# Snake instability of dark solitons in fermionic superfluids

A. Cetoli,<sup>1</sup> J. Brand,<sup>1</sup> R.G. Scott,<sup>2</sup> F. Dalfovo,<sup>2</sup> and L.P. Pitaevskii<sup>2,3</sup>

<sup>1</sup>*New Zealand Institute for Advanced Study and Centre for Theoretical Chemistry and Physics,  
Massey University, Private Bag 102904 NSMC, Auckland 0745, New Zealand*

<sup>2</sup>*INO-CNR BEC Center and Dipartimento di Fisica,*

*Università di Trento, Via Sommarive 14, I-38123 Povo, Italy*

<sup>3</sup>*Kapitza Institute for Physical Problems, ul. Kosygina 2, 119334 Moscow, Russia*

(Dated: June 21, 2021)

We present numerical calculations of the snake instability in a Fermi superfluid within the Bogoliubov-de Gennes theory of the BEC to BCS crossover using the random phase approximation complemented by time-dependent simulations. We examine the snaking behaviour across the crossover and quantify the timescale and lengthscale of the instability. While the dynamic shows extensive snaking before eventually producing vortices and sound on the BEC side of the crossover, the snaking dynamics is preempted by decay into sound due to pair breaking in the deep BCS regime. At the unitarity limit, hydrodynamic arguments allow us to link the rate of snaking to the experimentally observable ratio of inertial to physical mass of the soliton. In this limit we witness an unresolved discrepancy between our numerical estimates for the critical wavenumber of suppression of the snake instability and recent experimental observations with an ultra-cold Fermi gas.

PACS numbers: 67.85.De, 03.75.Lm, 03.75.Ss, 67.85.Lm

## I. INTRODUCTION

Solitons are a ubiquitous feature of fluid dynamics. In cold gases they are created in processes of non-equilibrium dynamics [1–8] such as a shock waves, phase and density imprinting, collisions between condensates, and moving obstacles, or a rapid quench through a superfluid phase transition [9–11], and may be observed long after the event if they are sufficiently stable. In strongly correlated Fermi superfluids, solitons provide a link between hydrodynamics and the poorly understood dynamics at interatomic length scales.

Dark and gray solitons are solitary wavefronts of reduced density that are stationary or propagate with a subsonic velocity on a background. In the context of superfluids, solitons are also called domain walls, as they are associated with a kink in the superfluid phase and thus separate domains of different phase. In weakly-interacting Bose-Einstein condensates (BECs) the study of dark and gray solitons has begun more than a decade ago [1, 2, 13]. While solitons live long enough to be observed, they are subject to a dynamical instability that leads to bending (snaking) of the depletion plane and eventually to the formation of vortex filaments or vortex rings [3, 14]. This process limits the lifetime of the soliton as the structure of the initial topological excitation is lost. The timescale of the decay is given by the excitation spectrum of this “snake instability”.

Ultra-cold atomic gases offer the opportunity to study the properties of solitons during the crossover from a weakly interacting BEC of pre-formed pairs of fermions to a strongly-correlated superfluid with unitarity-limited interactions and eventually to a Bardeen-Cooper-Schrieffer (BCS)-type superfluid with long-range pairing correlations [15, 16]. The crossover is controlled by the dimensionless parameter  $1/(k_F a)$ , where  $a$  is the s-

wave scattering length between Fermi atoms of opposite (pseudo) spin,  $k_F = (3\pi^2 n)^{1/3}$  the Fermi wavenumber, and  $n$  the density. While soliton properties in the BEC limit  $1/(k_F a) \gg 1$  are expected to match those of weakly interacting BECs that are well described by the Gross-Pitaevskii equation [17, 18], the situation is less clear but very interesting in the crossover region around the unitarity limit where  $1/(k_F a) = 0$ . The BCS limit  $1/(k_F a) \ll -1$  is currently not accessible to ultra-cold gas experiments. So far only the very recent experiment of Yefsah *et al.* has observed dark solitons in the crossover regime [8]. Here, solitons were created by phase imprinting and their subsequent dynamics in a prolate trap was observed, in order to obtain data for the ratio of inertial to physical mass. The solitons were seen to be remarkably stable against snaking; eventually, the signatures of the snaking instability appeared for certain trap aspect ratios.

A standard theoretical approach to modeling the BEC–BCS crossover is the Bogoliubov-de Gennes (BdG) crossover theory and its extensions based on diagrammatic many-body theory [15, 19]. Since there is no convenient small expansion parameter at unitarity, where the scattering length diverges and the particle separation  $n^{-1/3} \sim k_F^{-1}$  is the only available length scale, BdG crossover theory is non-perturbative and approximate in nature. The first numerical study of stationary solitons in 3D fermionic gases in this framework was done by Antezza *et al.* [20] (see also the work in 1D in Ref. [21]). Subsequent studies found numerical solutions for moving solitons and investigated their properties [22–24], but have been confined to purely one-dimensional dynamics. Of relevance to this paper are also general results on solitonic properties outside the approximate BdG crossover theory based on Landau quasiparticle theory [22], scaling analysis in the unitarity limit [23], and hydrodynamics

[25].

The properties of the system change upon changing the value the scattering length. In a pure BEC setting, the behavior of the snake instability is already known, and the excitation spectrum of the decay has been computed for different confinement potentials [26, 28]. More generally, the dispersion relation of the snaking process has been described in a work by Kamchatnov and Pitaevskii [25] with a hydrodynamical argument. This method can be also applied to fermionic superfluids, and gives a prediction for the excitation spectrum of the unstable modes responsible for the snaking in Fermi gases. Coming from a hydrodynamical approach, Kamchatnov and Pitaevskii's result is expected to be valid in the long wavelength limit.

Previous papers [22–24] have described the stability and the excitation spectrum of travelling dark solitons in superfluid Fermi gases. Here we wish to perform an analysis of the decay modes of stationary solitons in the context of the BdG theory. We first introduce the analytical argument of Ref. [25] in Sec. II. Then the excitation spectrum is studied with comprehensive numerical simulations, upon using a linear response approach in Sec. III and a time-dependent simulations in Sec. IV.

## II. HYDRODYNAMIC ARGUMENT

Let us consider a 3D soliton free to move along the  $x$  direction. This soliton can be seen as a surface in the Fermi gas with surface tension  $E_s$ . The motion happens according to the Newton's law of motion

$$m_s \frac{d^2 X}{dt^2} = F_s, \quad (1)$$

where  $X(t)$  is the  $x$  coordinate of a point on the depletion plane, and  $m_s = 2 \left. dE_s/d(V^2) \right|_{V=0}$  is the soliton's inertial mass. At the early stage of the snaking instability, the depletion plane would bend according to a sinusoidal perturbation

$$X(t) \propto \cos(qy - \omega_q t). \quad (2)$$

The surface tension appears as a force that tends to minimize the free energy of the system. More specifically, the force  $F_s$  acting on the soliton at the point  $X(t)$  depends on the curvature radius  $R$  of the plane itself

$$\begin{aligned} F_s &= \frac{E_s}{R} \\ R^{-1} &= \frac{d^2 X}{dy^2}. \end{aligned} \quad (3)$$

By substituting Eqs. (2) and (3) into Eq. (1) one obtains the hydrodynamic approximation for the instability dispersion [25]

$$\omega_q = \pm i \sqrt{E_s/|m_s|} q. \quad (4)$$

The value of  $\sqrt{E_s/|m_s|}$  can be found analytically at unitarity by using an argument based on the soliton's oscillation in a harmonic trap. This oscillation-based approach finds its utility when comparing the mean-field results to the data coming from experiments.

For this reason, let us call  $T_s$  the period of oscillation of the soliton in this type of potential, and  $T_{\text{trap}} = 2\pi/\omega_{\text{trap}}$  the inverse of the characteristic frequency of the trap. The value of  $m_s$  can be written in terms of  $T_s/T_{\text{trap}}$  by using the relation in Ref. [22, 23]

$$|m_s| = m|N_s| \left( \frac{T_s}{T_{\text{trap}}} \right)^2, \quad (5)$$

where  $m$  is the atomic mass. Equation (5) is completely generic, and it applies to solitons with any interaction strength.

At unitarity it is possible to estimate the energy of the soliton [23]  $E_s \propto \mu^2$ ; remembering that  $N_s = -\partial E_s/\partial \mu$

$$E_s = -\frac{N_s \mu}{2}. \quad (6)$$

By substituting Eqs. (6) and (5) into Eq. (4), after some calculations, we find

$$|\omega_q| \frac{\hbar}{E_F} = \sqrt{\frac{\mu}{E_F}} \left( \frac{T_{\text{trap}}}{T_s} \right) \frac{q}{k_F} \quad (7)$$

with  $E_F = \hbar^2 k_F^2/2m$ . At unitarity, equation (7) is an expression that conveniently relates the slope of the snaking excitation spectrum to the ratio  $T_{\text{trap}}/T_s$ . This ratio (related to the inertial mass ratio  $m_s/mN_s$  by Eq. (5)) is an experimentally measurable quantity.

In the unitarity limit, the BdG theory gives  $\mu/E_F \approx 0.6$ . In the same limit, both the BdG approach and analytical arguments [23] predict a period of oscillation as  $T_s/T_{\text{trap}} = \sqrt{3}$ , therefore

$$|\omega_q| \frac{\hbar}{E_F} = \sqrt{\frac{\mu}{E_F}} \frac{1}{\sqrt{3}} \frac{q}{k_F} \approx 0.45 \frac{q}{k_F}, \quad (8)$$

A different result is found if one assumes that the above hydrodynamic argument also applies to the recent experiment of Ref. [8]. The observed period of oscillation is much larger than the BdG prediction in the whole crossover region, with  $T_s/T_{\text{trap}} \approx 14$  at unitarity. Using this value in Eq. (7), together with the experimental value  $\mu/E_F \approx 0.36$ , one obtains

$$|\omega_q| \frac{\hbar}{E_F} \approx 0.043 \frac{q}{k_F}, \quad (9)$$

which implies a much slower decay rate. Even though the rate of instability,  $|\omega_q|$ , was not directly measurable in [8], the experiments seem to indicate that solitons having a long oscillation period have also a very long lifetime against snaking, in qualitative agreement with Eq. (7). The hydrodynamic arguments also suggests that both effects can be consistently attributed to a large mass ratio  $m_s/(mN_s)$ .

### III. RPA THEORY

The excitation spectrum of the snaking instability can be found by applying a transverse wave perturbation to the system. In the linear response approach one looks at the behavior of the system at small times after the perturbation has been applied. Within this approach, the poles of the static response function correspond to the normal modes of the system.

The entire excitation spectrum can in principle be found by computing the static response function  $\Pi(\omega_q, q)$  and by looking at the specific frequencies that make the denominator of  $\Pi$  vanish. It is worth noticing that the unstable modes of the snaking instability appear at imaginary frequencies.

In the following, we compute the response by using the random phase approximation (RPA) summation of diagrams [29–31], also called ring approximation.

#### A. Methodology

A many body system of spin 1/2 fermions with pairing is described by the Green's function

$$G(\mathbf{r}, t, \mathbf{r}', t') = \begin{pmatrix} \langle \hat{\psi}_\uparrow(\mathbf{r}, t) \hat{\psi}_\uparrow^\dagger(\mathbf{r}', t') \rangle & \langle \hat{\psi}_\uparrow(\mathbf{r}, t) \hat{\psi}_\downarrow(\mathbf{r}', t') \rangle \\ \langle \hat{\psi}_\downarrow(\mathbf{r}, t) \hat{\psi}_\uparrow^\dagger(\mathbf{r}', t') \rangle & \langle \hat{\psi}_\downarrow(\mathbf{r}, t) \hat{\psi}_\downarrow^\dagger(\mathbf{r}', t') \rangle \end{pmatrix}, \quad (10)$$

where  $\hat{\psi}_\sigma$  ( $\hat{\psi}_\sigma^\dagger$ ) is the destruction (creation) operator for the fermionic species  $\sigma = \downarrow, \uparrow$ .

In the Bogoliubov-de Gennes (BdG) theory the order parameter  $\Delta(\mathbf{r}, t)$  and the density  $n(\mathbf{r}, t)$  can be expressed in terms of the Bogoliubov amplitudes  $u(\mathbf{r}, t)$  and  $v(\mathbf{r}, t)$

$$\Delta = -g_{\text{eff}} \sum_j u_j v_j^*, \quad (11)$$

$$n = 2 \sum_j v_j v_j^*, \quad (12)$$

where the interaction strength  $g_{\text{eff}}$  is given by the renormalized value [15]

$$\frac{1}{g_{\text{eff}}} = \frac{m k_F}{4\pi\hbar^2} \frac{1}{k_F a} - \frac{1}{V} \sum_{\mathbf{k}} \frac{m}{\hbar^2 k^2}. \quad (13)$$

The value of  $a$  is the 3D scattering length describing the interactions between particles with different spins.

The BdG theory gives an explicit form of the Green's function using the Bogoliubov amplitudes  $u$  and  $v$  [32]

$$G(\mathbf{r}, \mathbf{r}', \omega_n) = \sum_j \frac{1}{i\omega_n - E_j/\hbar} \begin{pmatrix} u_j(\mathbf{r}) \\ v_j(\mathbf{r}) \end{pmatrix} \begin{pmatrix} u_j^*(\mathbf{r}') & v_j^*(\mathbf{r}') \end{pmatrix} + \sum_j \frac{1}{i\omega_n + E_j/\hbar} \begin{pmatrix} -v_j^*(\mathbf{r}) \\ u_j^*(\mathbf{r}) \end{pmatrix} \begin{pmatrix} -v_j(\mathbf{r}') & u_j(\mathbf{r}') \end{pmatrix} \quad (14)$$

where  $\omega_n = (2n+1)\pi/\beta\hbar$  ( $n$  integer) is a fermionic Matsubara frequency. The static problem for the Bogoliubov

amplitudes is solved by finding the solutions of the equations

$$\begin{pmatrix} -\frac{\hbar^2 \nabla^2}{2m} - \mu & \Delta \\ \Delta^* & \frac{\hbar^2 \nabla^2}{2m} + \mu \end{pmatrix} \begin{pmatrix} u_j \\ v_j \end{pmatrix} = E_j \begin{pmatrix} u_j \\ v_j \end{pmatrix}, \quad (15)$$

where  $E_j$  are the excitations energies of the Bogoliubov amplitudes.

We are interested in the response of the pair fluctuation  $\hat{\psi}_\downarrow(\mathbf{r}t)\hat{\psi}_\uparrow(\mathbf{r}t)$ . For this purpose, let us define

$$\begin{aligned} \hat{\chi}(\mathbf{r}, t) &= \hat{\psi}_\downarrow(\mathbf{r}, t) \hat{\psi}_\uparrow(\mathbf{r}, t) \\ \hat{\chi}^\dagger(\mathbf{r}, t) &= \hat{\psi}_\uparrow^\dagger(\mathbf{r}, t) \hat{\psi}_\downarrow^\dagger(\mathbf{r}, t), \end{aligned} \quad (16)$$

and introduce the vector

$$\xi(\mathbf{r}, t) = \begin{pmatrix} \langle \hat{\chi}(\mathbf{r}, t) \rangle \\ \langle \hat{\chi}^\dagger(\mathbf{r}, t) \rangle \end{pmatrix} \quad (17)$$

The time-dependence of the vector in Eq. (16) can be studied in the linear approximation. In order to study the snaking instability we apply a small transversal perturbation to the depletion plane of a soliton, which has the form

$$e^{i\mathbf{q}_y \mathbf{y} + i\mathbf{q}_z \mathbf{z}} \phi_0, \quad (18)$$

with  $\phi_0$  a two-component vector. The result in the RPA approximation is [30, 33]

$$\delta\xi(x, q_y, q_z, t) = \int d\omega e^{i\omega t} \int dx' \Pi^{\text{RPA}}(x, x', q_y, q_z, \omega) \phi_0 \quad (19)$$

where  $x$  is the coordinate on the depletion plane of the soliton, and  $q_y, q_z$  are the wavenumber of the transversal perturbation. The response function is

$$\Pi^{\text{RPA}}(x, x', q_y, q_z, \omega) = \int dx'' [\mathbf{1}_{x, x''} - g_{\text{eff}} \Pi_0(x, x'', q_y, q_z, \omega)]^{-1} \Pi_0(x'', x', q_y, q_z, \omega), \quad (20)$$

with  $g_{\text{eff}}$  being the renormalized interaction,

$$\mathbf{1}_{x, x''} = \begin{pmatrix} \delta(x - x'') & 0 \\ 0 & \delta(x - x'') \end{pmatrix}, \quad (21)$$

and

$$\Pi_0 = \begin{pmatrix} \langle \hat{\chi} \hat{\chi}^\dagger \rangle & \langle \hat{\chi} \hat{\chi} \rangle \\ \langle \hat{\chi}^\dagger \hat{\chi}^\dagger \rangle & \langle \hat{\chi}^\dagger \hat{\chi} \rangle \end{pmatrix}. \quad (22)$$

Here, expectation values are evaluated as averages corresponding to sums over the quasiparticle amplitudes calculated with the stationary BdG equations. The same expression can be given in terms of the Green's function of Eq. (10)

$$\Pi_0 = \begin{pmatrix} -G_{00} G'_{11} & -G_{01} G'_{01} \\ -G_{10} G'_{10} & -G_{11} G'_{00} \end{pmatrix}, \quad (23)$$

which can eventually be expressed by using the Bogoliubov amplitudes. The details of this calculation are presented in Appendix A.

Finally, the poles of the system are given by the condition

$$\det(\mathbf{1}_{x,x''} - g_{\text{eff}} \Pi_0(q, \omega)_{x,x''}) = 0, \quad (24)$$

with  $\Pi_0(q, \omega)$  being a tensor in the coordinates  $x$  and  $x''$ . The resonant energies of the system are given by the poles of  $\Pi^{\text{RPA}}$ .

These poles can be complex. For definiteness, let us use  $\Omega$  for the real part and  $\gamma$  for the imaginary part, so that

$$\omega = \Omega + i\gamma. \quad (25)$$

For each value of  $q_y$  and  $q_z$  these poles must satisfy the relation

$$\det[\mathbf{1} \lambda - g_{\text{eff}} \Pi_0(q_y, q_z, \Omega_{q_y, q_z} + i\gamma_{q_y, q_z})] = 0, \quad (26)$$

with  $\lambda = 1$ . Notice that, for given frequency  $\Omega_{q_y, q_z} - i\gamma_{q_y, q_z}$ ,  $g_{\text{eff}} \Pi_0$  is a matrix in the 2-dimensional space defined in Eq. (17), so that Eq. (26) is equivalent to finding a vector  $|\lambda\rangle$  such that

$$g_{\text{eff}} \Pi_0(q_y, q_z, \Omega_{q_y, q_z} + i\gamma_{q_y, q_z})|\lambda\rangle = |\lambda\rangle. \quad (27)$$

In other words, it is possible to diagonalize  $g_{\text{eff}} \Pi_0$  and search for the eigenvalues equal to 1 for each frequency  $\Omega_{q_y, q_z} + i\gamma_{q_y, q_z}$ . The eigenvectors corresponding to the eigenvalue 1 are the ones that provide the resonances.

## B. Results

For plotting the snake instability spectrum we seek to find the complex values for small values of  $q$ . In the RPA analysis we see that the spectrum is purely imaginary ( $\Omega = 0$ ) close to  $q = 0$ . The results are plotted in Fig. 1 for various values of the interaction  $1/(k_F a)$ .

The search algorithm discretizes the plane and looks at different combinations of energy and  $q$ ; when a unit eigenvalue ( $\lambda = 1$ ) is found we plot the corresponding resonance value. At our highest resolution, we have chosen an energy step of  $0.001 E_F$  and a step for  $q$  of  $0.065 k_F$ . We have chosen the resolution in the energy as the error in the determination of the poles. In these calculations we have set an energy cutoff of  $E_C = 20 E_F$ ; larger cutoffs would imply extremely time consuming calculations.

We point out that a cutoff effect in the RPA calculations seems to be relevant on the BEC side of the crossover. As a consequence, for  $1/(k_F a) > 0.2$  our RPA results do not show any excitation poles in the range predicted by the hydrodynamical argument, and convergence with the results in Ref. [26] is not obtained.

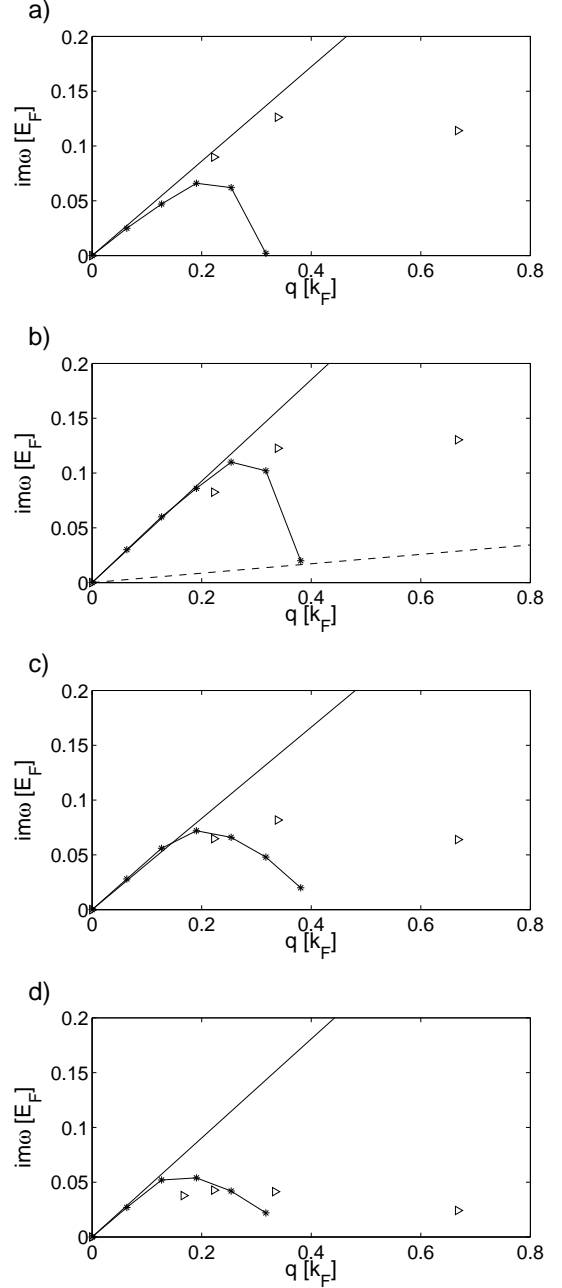


FIG. 1: Rate of snake instability of a dark soliton as a function of the wavevector of the snaking oscillation. Stars joined by solid lines correspond to the resonant poles calculated with RPA for  $1/(k_F a) = 0.2(a), 0(b), -0.5(c), -0.75(d)$ . The numerical error for these points is about  $0.001 E_F$ . Triangles correspond to the growth rate obtained in the time-dependent BdG simulations. The solid straight line in each panel is the hydrodynamic prediction (4), valid in the small  $q$  limit, with  $E_s$  and  $m_s$  obtained from the stationary BdG equations. At unitarity (panel (b)) this line coincides with Eq. (8), while the dashed line represents Eq. (9), which is the same hydrodynamic relation, but using the experimental value for the chemical potential and the period of oscillation of solitons as measured in [8].

	$ \text{Im}(\omega_q) /q \text{ } [v_f]$	
$1/k_F a$	Hydrod.	RPA
0.2	0.215	$0.2 \pm 0.01$
0	0.232	$0.23 \pm 0.01$
-0.5	0.208	$0.22 \pm 0.01$
-0.75	0.226	$0.21 \pm 0.01$

Table 1: Slope of the dispersion law of the unstable excitation mode for different interaction strengths. The hydrodynamic prediction corresponds to the ratio  $E_s/m_s$  as in Eq.(4); this ratio is computed by using the method of Ref.[23]. The RPA values are calculated from the numerical RPA results in Fig. 1, in the low  $q$  limit.

At low  $q$  the RPA results are in agreement with Eq. (4), as shown in Table 1. This is a nontrivial result, and we stress this is the first microscopic numerical check of the hydrodynamic argument by Kamchatnov and Pitaevskii. The RPA results deviate from the linear slope downward at large  $q$ .

#### IV. TIME-DEPENDENT SIMULATIONS

The time-dependent Bogoliubov-de Gennes (TDBdG) equations are numerically solved to further study the snaking instability. We simulate the time evolution of the soliton for a set of values of the interaction strength in the crossover. As discussed previously, the soliton itself is an unstable solution of the stationary BdG equations; for this reason the snaking has to be induced by applying a small initial perturbation to the system.

##### A. Methodology

The functions  $u$  and  $v$  solve the equation of motion [34]

$$\begin{pmatrix} -\frac{\hbar^2 \nabla^2}{2m} - \mu & \Delta \\ \Delta^* & \frac{\hbar^2 \nabla^2}{2m} + \mu \end{pmatrix} \begin{pmatrix} u_j(\mathbf{r}, t) \\ v_j(\mathbf{r}, t) \end{pmatrix} = i \hbar \partial_t \begin{pmatrix} u_j(\mathbf{r}, t) \\ v_j(\mathbf{r}, t) \end{pmatrix}. \quad (28)$$

We choose to confine the system in a box with periodic boundary conditions along the transverse directions  $y$  and  $z$  and Dirichlet boundary conditions in the longitudinal  $x$  direction. We keep the box size in the  $x$  and  $z$  directions fixed ( $30k_F^{-1}$  and  $10k_F^{-1}$ , respectively) while varying the size in the transverse  $y$  direction,  $L_y$ , in the range from 10 to  $40k_F^{-1}$ ; this is the direction along which we perturb the soliton to obtain snaking. The regularization procedure needed to remove the ultraviolet divergences in the BdG equations is the same as the one used before in the RPA method. In the time-dependent simulations we use the cutoff energy  $E_c = 50E_F$  for pos-

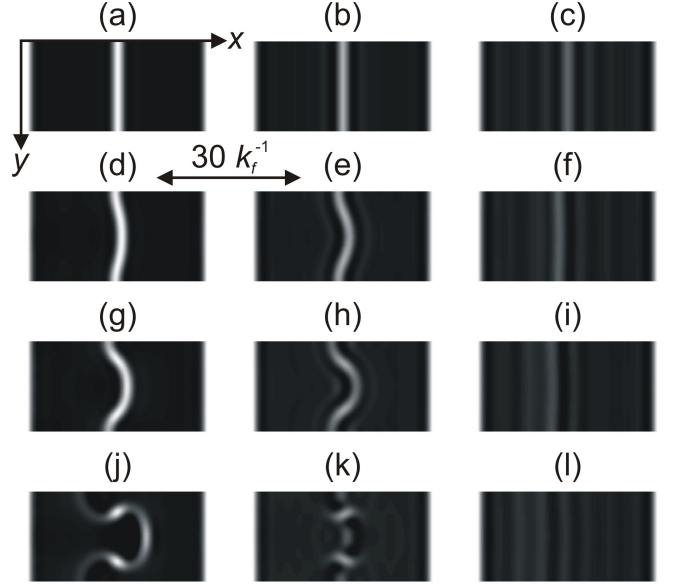


FIG. 2: Decay of the soliton for various values of the interaction strength  $1/k_F a$  in the BCS regime. The column on the left depicts the evolution of the soliton at unitarity, the middle column is about  $1/k_F a = -0.5$  while the rightmost column describes the case  $1/k_F a = -1$ . The time evolution at unitarity is presented at the times  $0\hbar/E_F$  (a),  $34\hbar/E_F$  (d),  $43\hbar/E_F$  (g) and  $54\hbar/E_F$  (j); for the middle column the times are  $0\hbar/E_F$  (b),  $67\hbar/E_F$  (e),  $79\hbar/E_F$  (h) and  $90\hbar/E_F$  (k), while at  $1/k_F a = -1$  the evolution is shown for  $0\hbar/E_F$  (c),  $157\hbar/E_F$  (f),  $180\hbar/E_F$  (i) and  $200\hbar/E_F$  (l).

itive values of the scattering length and  $E_c = 30E_F$  for negative values.

We first prepare the soliton as a stationary solution of the BdG equations and then we modify it by imposing a tiny phase shift  $\delta\phi = 0.02\pi \sin(2\pi y/L_y)$  on  $\Delta$  at the left of the soliton plane (for  $x < 0$ ). This slightly perturbed state is used as the initial state of the TDBdG simulation, at  $t = 0$ . The small perturbation acts as a seed for the snaking of the soliton. The characteristic wavenumber of the perturbation is  $q = 2\pi/L_y$ . The position  $x(t)$  of the nodal plane is then measured at  $y = L_y/2$  and  $z = 0$ , and fitted with the exponential law  $x(t) \propto \exp(\gamma t)$ .

##### B. Results

The deformation of the soliton grows exponentially at short times and eventually cause the soliton to decay into vortices, as shown in Fig 2 [35]. The values of  $\gamma$  are given in Fig. 1 as a function of  $q$  and for different values of the interaction strength. In the long wavelength limit, the TDBdG points approach the hydrodynamic law (4), while bending downward at larger  $q$ , similarly to the previous RPA results. The two theories differ in the way they deviate from the linear slope. Near unitarity, the RPA calculations seem to better agree with the hydrodynamical approach than TDBdG. An explanation might



lay in the use of Dirichlet boundary conditions in the time-dependent approach. Indeed we have checked that using a box with hard walls instead of periodic boundary conditions can lower the slope of the excitation spectrum also in RPA calculations.

This effect, however, does not explain the large discrepancy between the RPA and TDBdG at large  $q$ , where the RPA points bend down much faster. On the one hand, this could be due to the role of the cutoff energy  $E_c$ , which is smaller in the RPA calculations than in TDBdG, hence limiting the convergence toward cutoff-independent results. On the other hand, the discrepancy at large  $q$  may be related to nonlinear effects present in the TDBdG calculation but absent in RPA, which is a linear response theory.

It is worth noticing that, for  $1/k_F a = -1$ , the TDBdG simulations give no evidence of snaking instability for any value of  $q$ , the result of the evolution being only the emission of phonons, as shown in the right column of Fig. 2. This can be explained by considering the decay process discussed in Ref. [24]: on the BCS side of the crossover, the soliton can decay due to pair-breaking when moving at a speed larger than a critical one, eventually emitting phonons. The critical velocity becomes vanishingly small in the BCS limit. For our simulation this implies that the motion induced by the initial phase shift reaches soon the condition of critical velocity, before developing the snaking instability.

## V. DISCUSSIONS AND CONCLUSIONS

Our calculations assume the system to be uniform in the transverse direction. In trapped gases, the snaking instability can be suppressed if the superfluid is tightly confined in the transverse direction. It makes sense to calculate the effect of the transverse confinement in terms of the relevant parameter

$$\eta = \frac{\mu}{\hbar\omega_\perp} \quad (29)$$

where  $\mu$  is the chemical potential and  $\omega_\perp$  is the harmonic trapping frequency. We consider both the BEC and the unitary Fermi gas in the Thomas-Fermi approximation, where the density profile is determined by

$$\mu = \frac{1}{2}m\omega^2\rho^2 + \mu_{\text{loc}}(n) \quad (30)$$

where  $\mu_{\text{loc}}(n)$  the chemical potential of a uniform gas of density  $n$ , fixed by the equation of state, and  $\rho$  is the transverse (radial) coordinate. The Thomas-Fermi radius  $\rho_{\text{TF}}$  is determined by  $\mu_{\text{loc}} = 0$ , yielding  $\rho_{\text{TF}}^2 = 2\mu/(m\omega^2)$ .

In the BEC case, defining the healing length as  $\xi = \hbar/\sqrt{2m\mu_{\text{loc}}}$  we can calculate the dimensionless number of healing lengths across the condensate,

$$N_\xi = 2 \int_0^{\rho_{\text{TF}}} \frac{d\rho}{\xi} = \pi \eta \quad (31)$$

where the second equality follows by virtue of the Thomas-Fermi approximation and the details of the equation of state are irrelevant. In Murychev et al. [26], the critical value  $\eta_c \approx 2.4$  was determined numerically for suppression of the snaking instability for  $\eta < \eta_c$ . This corresponds to a value of  $N_\xi^c \approx 7.5$ . Numerical calculations in a two-dimensional channel with hard walls give a similar value,  $N_\xi^c \approx 6$  [28]. These values can be compared with calculations of the homogeneous and infinite soliton plane, which has a long-wavelength instability at wavenumber  $k_c = 1/\sqrt{2}\xi$  [26], corresponding to a wavelength of  $2\pi/k_c = 2\sqrt{2} \approx 8.9$ , close enough to the above values. We conclude that snaking occurs when a full unstable wavelength fits onto the transverse Thomas-Fermi profile.

As shown in Appendix B and Fig. 3, the healing length is also a relevant length scale in the crossover up to the unitarity regime, and seems to set the relevant length scale for short-wavelength suppression of the snaking instability, although the available numerical data is not entirely conclusive.

For a unitary Fermi gas the relevant length unit is the inverse Fermi wave number  $k_F^{-1} = (2\pi^2 n)^{-1/3}$  and  $\xi = 0.7 k_F^{-1}$ . Using the equation of state  $\mu_{\text{loc}}(n) = (1 + \beta) \hbar^2 k_F^2 / 2m$ , we obtain

$$\begin{aligned} N_{k_F^{-1}} &= 2 \int_0^{\rho_{\text{TF}}} k_F d\rho \\ &= -\frac{\pi}{\sqrt{1+\beta}} \eta \approx 5 \eta \end{aligned} \quad (32)$$

where  $1 + \beta \approx 0.4$  was used [27]. The numerical data we have obtained suggests a critical wavenumber of 0.5 to 1.0  $k_F$ , which would suggest a length scale of 6 to 12  $k_F^{-1}$ , or a value of  $\eta_c^{\text{BdG}} \approx 1.5$  to 3. However, the recent MIT experiment reports  $\eta_c \approx 25$  corresponding to  $N_{k_F^{-1}} \approx 125$ . This is obviously a significant discrepancy. The solitons are stable in a much wider regime in experiment than would be expected from the BdG calculations and this demands further theoretical investigations.

To conclude, we have performed a comprehensive analysis of the snake instability across the BEC-BCS crossover within the mean-field BdG approximations, both by using a time-dependent approach and a response function-based method. In our analysis, we have seen the snake instability to occur in the crossover, but may be preceded by decay into sound in the deep BCS regime.

In the long wavelength limit mean-field hydrodynamic arguments predict that the timescale of the decay is set by the soliton energy and mass. Our BdG calculations well agree with this prediction. However, for smaller wavelengths in the BCS regime there is a departure from this behavior; the departure might be due to pair-breaking or boundary conditions.

On the other hand, the timescales measured in experiment are much longer. If these experimental results are confirmed other effects must also be taken into account to accurately describe the snaking in the crossover regime.

### Acknowledgments

We thank Sandro Stringari and Martin Zwierlein for insightful discussions. AC is grateful to the Wenner-Gren foundations for financial support. The work is also supported by ERC through the QGBE grant and by Provincia Autonoma di Trento. RS is grateful for the use of the AURORA supercomputing facilities in Trento.

### Appendix A: The renormalization

The un-renormalized response function  $\Pi^{\text{RPA}}$  in the RPA approximation is

$$\begin{aligned} \Pi^{\text{RPA}}(x, x', q_y, q_z, \omega) &= \int dx'' [\mathbf{1}_{x, x''} \\ &\quad - g \Pi_0(x, x'', q_y, q_z, \omega)]^{-1} \Pi_0(x'', x', q_y, q_z, \omega) \end{aligned} \quad (33)$$


---

where  $g = 4\hbar^2\pi a_s/m$  the “bare” interaction and,  $\Pi_0$  is the lowest order response function given by Eq. (22). The expression for  $\Pi_0$  can be evaluated by using the Wick’s theorem. For example, at  $T = 0$

$$\begin{aligned} \langle \hat{\chi} \hat{\chi}^\dagger \rangle(x, x', q_y, q_z) &= \frac{1}{\beta\hbar} \sum_{\omega_l, k_x, k_y} \langle \hat{\psi}_\downarrow(x, k_x + q_y, k_y + q_z, \omega_n + \omega_l) \hat{\psi}_\uparrow^\dagger(x, k_x + q_y, k_y + q_z, \omega_n + \omega_l) \\ &\quad \times \hat{\psi}_\uparrow^\dagger(x', k_x, k_y, \omega_n) \hat{\psi}_\downarrow(x', k_y, k_z, \omega_n) \rangle \\ &= -G_{00} G'_{11} \\ &= -\frac{1}{\beta\hbar} \sum_{\omega_l, k_x, k_y} \langle \hat{\psi}_\uparrow(x, k_x + q_y, k_y + q_z, \omega_n + \omega_l) \hat{\psi}_\uparrow^\dagger(x', k_x + q_y, k_y + q_z, \omega_n + \omega_l) \rangle \\ &\quad \times \langle \hat{\psi}_\downarrow^\dagger(x', k_x, k_y, \omega_n) \hat{\psi}_\downarrow(x, k_y, k_z, \omega_n) \rangle \\ &= -\frac{1}{\beta\hbar} \sum_{\omega_l, k_x, k_y} G_{00}(x, x', k_x + q_y, k_y + q_z, \omega_n + \omega_l) G_{11}(x', x, k_y, k_z, \omega_n) \\ &= -\sum_{\eta, \eta'} \left\{ u_\eta(x) u_\eta^*(x') u_{\eta'}^*(x') u_{\eta'}(x) \frac{1}{\hbar^{-1}(E_\eta + E_{\eta'}) - \omega + i\epsilon} \right. \\ &\quad \left. + v_\eta(x) v_\eta^*(x') v_{\eta'}^*(x') v_{\eta'}(x) \frac{1}{\hbar^{-1}(E_\eta + E_{\eta'}) + \omega + i\epsilon} \right\}, \end{aligned} \quad (34)$$


---

where the index  $\eta$  is a vector that contains the information over the wave vectors and  $\omega$ :

$$\begin{aligned} \eta &= (k_x, k_y, \omega_n) \\ \eta' &= (k_x + q_x, k_y + q_y, \omega_n + \omega_l). \end{aligned} \quad (35)$$

Equation (22) can be rewritten as

$$\Pi_0 = \begin{pmatrix} -G_{00} G'_{11} & -G_{01} G'_{01} \\ -G_{10} G'_{10} & -G_{11} G'_{00} \end{pmatrix}, \quad (36) \quad \text{and}$$

where the prime over  $G'$  inverts the coordinates

$$\begin{aligned} G_{\alpha\beta} &= G_{\alpha\beta}(x, x', q_y, q_z) \\ G'_{\alpha\beta} &= G_{\alpha\beta}(x', x, q_y, q_z), \end{aligned} \quad (37)$$

$$\begin{aligned}
G_{\alpha\beta}(x_1, x_2, q_y, q_z) G_{\gamma\delta}(x_3, x_4, q_y, q_z) &= \sum_{\eta, \eta'} \left\{ \chi_{\eta}^{(\alpha)}(x_1) (\chi_{\eta}^{(\beta)})^*(x_2) (\tilde{\chi}_{\eta'}^{(\gamma)})^*(x_3) \tilde{\chi}_{\eta'}^{(\delta)}(x_4) \right. \\
&\quad \times \frac{1}{\hbar^{-1}(E_{\eta} + E_{\eta'}) - \omega + i\epsilon} \\
&\quad + \tilde{\chi}_{\eta}^{(\alpha)}(x_1) (\tilde{\chi}_{\eta}^{(\beta)})^*(x_2) (\chi_{\eta'}^{(\gamma)})^*(x_3) \chi_{\eta'}^{(\delta)}(x_4) \\
&\quad \left. \times \frac{1}{\hbar^{-1}(E_{\eta} + E_{\eta'}) + \omega + i\epsilon} \right\}. \tag{38}
\end{aligned}$$

with

$$\chi_{\eta}(x) = \begin{pmatrix} u_{\eta}(x) \\ -v_{\eta}(x) \end{pmatrix}, \tag{39}$$

and

$$\tilde{\chi}_{\eta}(x) = \begin{pmatrix} v_{\eta}^*(x) \\ u_{\eta}^*(x) \end{pmatrix}. \tag{40}$$

The energy  $E_{\eta}$  is the Bogoliubov energy for the state  $\eta$ . The index  $\eta$  is given by a set of three numbers: the number of the longitudinal excitation energy and the transverse excitation numbers  $q_x$  and  $q_y$ . A standard renormalization procedure prescribes to use the term  $G_{11} G'_{00} - V^{-1} \sum m/\hbar^2 k^2$  instead (and similarly for the other term).

Eventually the equation that gives the poles, in the cutoff independent form, is

$$\det \begin{pmatrix} -\frac{1}{g} - G_{00} G'_{11} + \frac{1}{V} \sum \frac{m}{\hbar^2 k^2} & -G_{01} G'_{01} \\ -G_{10} G'_{10} & -\frac{1}{g} - G_{11} G'_{00} + \frac{1}{V} \sum \frac{m}{\hbar^2 k^2} \end{pmatrix} = 0. \tag{41}$$

For a system of boson the natural length is the “healing length”

Notice that Eq. (41) can be rewritten as

$$\det \begin{pmatrix} -G_{00} G'_{11} - \frac{1}{g_{\text{eff}}} & -G_{01} G'_{01} \\ -G_{10} G'_{10} & -G_{11} G'_{00} - \frac{1}{g_{\text{eff}}} \end{pmatrix} = 0, \tag{42}$$

which is the expression used in the text in Eq. (24).

## Appendix B

As was first shown in Ref. [36], the snake instability is a long wavelength phenomenon that disappears at shorter wavelengths: the soliton’s imaginary excitation spectrum exists up to a maximum wavenumber. In a BEC, this critical wavenumber is the inverse of the healing length. We seek to compare our results to the natural characteristic lengths of the system in the BEC and BCS regimes.

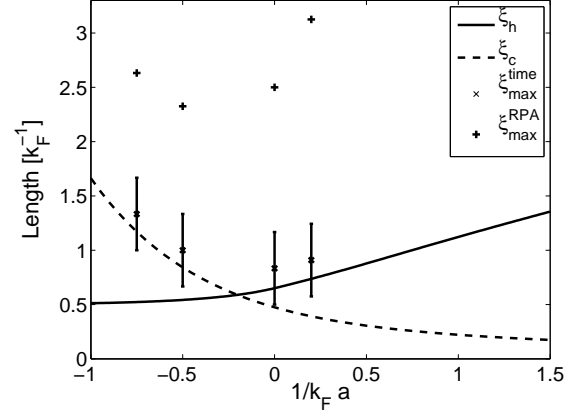


FIG. 3: Characteristic lengths in the BCS regime ( $\xi_c$ ) and BEC regime ( $\xi_h$ ) as a function of  $1/(k_F a)$ , as computed with Eqs. (46) and (43). The values of  $\xi_{\text{max}}^{\text{time}}$  and  $\xi_{\text{max}}^{\text{RPA}}$  are taken from the time-dependent approach by looking at the longest perturbation wavelength that gives an imaginary spectrum.

$$\xi_h = \frac{\hbar}{\sqrt{2m\mu_B}}, \tag{43}$$

where  $\mu_B$  is the boson chemical potential. From Ref. [32]

$$\mu_B = \Delta_0 + 2\mu_{BCS}, \tag{44}$$

where  $\mu_{BCS}$  is the fermionic chemical potential from the BdG equations. Therefore

$$\xi_h = \frac{\hbar}{\sqrt{2m(\Delta_0 + 2\mu_{BCS})}}. \tag{45}$$

where  $\Delta_0$  is the pairing energy. On the other hand, the characteristic length in the BCS regime is the “coherence length”

$$\xi_c = \frac{\hbar v_F}{\pi \Delta_0}, \tag{46}$$

The values for  $\mu_{BCS}$  and  $\Delta_0$  for the infinite and uniform as a function of the interaction  $1/k_F a$  can be found



by following the method in Ref. [37]. The result is plotted in Fig. 3.

Only in the deep BCS and BEC limit these two quan-

tities become experimentally relevant. It is however interesting to see that the characteristic length seems to increase in both limits.

- 
- [1] S. Burger, K. Bongs, S. Dettmer, W. Ertmer, and K. Sengstock, *Phys. Rev. Lett.*, **83**, 25 (1999).
  - [2] J. Denschlag, J.E. Simsarian, D.L. Feder, Charles W. Clark, L.A. Collins, J. Cubizolles, L. Deng, E. W. Hagley, K. Helmerson, W. P. Reinhardt, S.L. Rolston, B.I. Schneider, W.D. Phillips *Science* **287**, 97 (2000).
  - [3] Z. Dutton, M. Budde, C. Slowe, L. Vestergaard Hau, *Science* **293**, 663 (2001).
  - [4] P. Engels, and C. Atherton, *Phys. Rev. Lett.* **99**, 160405 (2007).
  - [5] C. Becker et al. *Nat. Phys.* **4**, 496 (2008).
  - [6] I. Shomroni, E. Lahoud, S. Levy, J. Steinhauer, *Nat. Phys.* **5**, 193 (2009).
  - [7] C. Hamner, J. J. Chang, P. Engels, M. A. Hoefer, *Phys. Rev. Lett.* **106**, 065302 (2011).
  - [8] T. Yefsah et al., *Nature* **499**, 426 (2013).
  - [9] W. Zurek, *Phys. Rev. Lett.*, **102**, 105702 (2009).
  - [10] T. Kibble, *Physics Today*, **60**, 47 (2007).
  - [11] G.Lamporesi, S.Donadello, S.Serafini, F.Dalfovo, G.Ferrari, *Nat. Phys.* **9**, 656 (2013).
  - [12] A. Bulgac, Y.-L. Luo, and K. Roche, *Phys. Rev. Lett.* **108**, 150401 (2012).
  - [13] W. P. Reinhardt and C. W. Clark *J. Phys. B.* **30**, L785-L789 (1997).
  - [14] B. P. Anderson, P. C. Haljan, C. A. Regal, D. L. Feder, L. A. Collins, C. W. Clark, and E. A. Cornell, *Phys. Rev. Lett.* **86**, 2926 (2001).
  - [15] S. Giorgini, L. Pitaevskii, S. Stringari, *Rev. Mod. Phys.* **80**, 4 (2008).
  - [16] W. Ketterle and M. W. Zwierlein, *Ultracold Fermi Gases*, Proceedings of the International School of Physics "Enrico Fermi", Course CLXIV, Varenna, 20 - 30 June 2006, edited by M. Inguscio, W. Ketterle, and C. Salomon (IOS Press, Amsterdam) 2008, pp. 95-287; *Rivista del Nuovo Cimento* **31**, 247 (2008).
  - [17] J. Brand, L. D. Carr, and B. P. Anderson, *Emergent Nonlinear Phenomena in Bose-Einstein Condensates* (2008 Berlin: Springer) chapter 8, p 157.
  - [18] L. D. Carr and J. Brand, *Emergent Nonlinear Phenomena in Bose-Einstein Condensates* (2008 Berlin: Springer), chapter 7, p 133.
  - [19] A. Spuntarelli, P. Pieri, and G.C. Strinati, *Physics Reports* **488**, 111-167 (2010).
  - [20] M. Antezza et al, *Phys. Rev. A* **76**, 043610 (2007).
  - [21] J. Dziarmaga, K. Sacha, *arxiv:cond-mat/0407585*.
  - [22] R. G. Scott, F. Dalfovo, L. P. Pitaevskii, and S. Stringari *Phys. Rev. Lett.* **106**, 185301 (2011).
  - [23] R. Liao and J. Brand *Phys. Rev. A* **83**, 041604(R) (2011).
  - [24] R. G. Scott et al, *New J. Phys.* **14**, 023044 (2012).
  - [25] A.M. Kamchatnov and L.P. Pitaevskii *Phys. Rev. Lett.*, **100**, 160402 (2008).
  - [26] A.E. Muryshev et al., *Phys. Rev. A* **60**, 4 (1999).
  - [27] D. Blume, J. von Stecher, and C. H. Greene, *Phys. Rev. Lett.* **99**, 233201 (2007).
  - [28] J.Brand and W.P Reinhardt, *Phys. Rev. A* **65**, 043612 (2002).
  - [29] A. Leggett, *Phys. Rev.* **147**, 1 (1966)
  - [30] G.M. Bruun and B.R. Mottleson, *Phys. Rev. Lett.* **87**, 27 (2001).
  - [31] A. Minguzzi et al., *Eur. Phys. J. D* **17**, 49-55 (2001).
  - [32] P. Pieri and G.C. Strinati, *Phys. Rev. Lett.*, Vol. **91**, 030401 (2003).
  - [33] A.L. Fetter and J.D. Walecka, *Quantum Field Theory of Many-Particle Systems*, McGraw-Hill (1971)
  - [34] K.J. Challis, R.J. Ballagh, and C.W. Gardiner *Phys. Rev. Lett.* **98**, 4 (2007).
  - [35] The same decay mechanism has been seen in the numerical simulations of a Fermi superfluid at unitarity by Bulgac et al., *arXiv:1306.4266*. In that case, due to the different geometry, the snaking instability produces vortex rings instead of straight vortex lines, but the timescale of the process is compatible with our results.
  - [36] E.A. Kuznetsov and S.K. Turitsyn, *Sov. Phys. JETP* **67**, 1583 (1988).
  - [37] R. Combescot, M.Yu. Kagan and S. Stringari, *Phys. Rev. A* **74**, 042717 (2006).